

Two-site fluctuations and multipolar intersite exchange interactions in strongly correlated systems

L. V. Pourovskii*

*Centre de Physique Théorique, École Polytechnique, CNRS, Université Paris-Saclay, 91128 Palaiseau, France;**Collège de France, 11 place Marcelin Berthelot, 75005 Paris, France;**and Materials Modeling and Development Laboratory, National University of Science and Technology "MISIS," Moscow, Russia*

(Received 16 March 2016; revised manuscript received 10 August 2016; published 8 September 2016)

An approach is proposed for evaluating dipolar and multipolar intersite interactions in strongly correlated materials. This approach is based on the single-site dynamical mean-field theory (DMFT) in conjunction with the atomic approximation for the local self-energy. Starting from the local-moment paramagnetic state described by DMFT, we derive intersite interactions by considering the response of the DMFT grand potential to small fluctuations of atomic configurations on two neighboring sites. The present method is validated by applying it to one-band and two-band e_g Hubbard models on the simple-cubic $3d$ lattice. It is also applied to study the spin-orbital order in the parent cubic structure of ternary chromium fluoride KCrF_3 . We obtain the onset of a G-type antiferro-orbital order at a significantly lower temperature compared to that in real distorted KCrF_3 . In contrast, its layered A-type antiferromagnetic order and Néel temperature are rather well reproduced. The calculated full Kugel-Khomskii Hamiltonian contains spin-orbital coupling terms inducing a misalignment in the antiferro-orbital order upon the onset of antiferromagnetism.

DOI: [10.1103/PhysRevB.94.115117](https://doi.org/10.1103/PhysRevB.94.115117)**I. INTRODUCTION**

Magnetic and orbital-ordering phenomena in strongly correlated materials have been a hot topic in condensed matter research for many years. In particular, transition-metal (TM) oxides and fluorides have attracted a lot of attention due to a complex interplay of their spin and orbital orderings [1]. More recently, a lot of research has been focused on the lanthanide and actinide compounds exhibiting ordering of high-ranking multipoles, e.g., CeB_6 [2,3], actinide dioxides AO_2 ($A = \text{U}, \text{Np}, \text{and Pu}$) [4], and URu_2Si_2 , where the nature of the “hidden-order” phase is still hotly debated [5]. Experimental determination of multipole-ordered structures is a complicated task, because the conventional neutron diffraction method is often not applicable in this case [4].

Dipolar and multipolar moments in those materials are carried by localized shells of correlated d and f electrons. First-principles description of such strongly correlated compounds is nowadays possible using a combination [6,7] of density-functional-theory (DFT) band structure techniques with the dynamical mean-field theory (DMFT) treatment [8] of correlated electrons. This approach is particularly efficient in capturing the high-temperature symmetry-unbroken state. There are no principal limitations for applications of the same method to symmetry-broken ordered phases. However, the typical low ordered temperatures and low symmetries of those phases as well as a vast configuration space of possible ordered states render direct predictive DFT+DMFT calculations in this case rather difficult. Moreover, the single-site DMFT method suffers from the usual mean-field drawbacks overestimating ordering temperatures, especially, for low-dimensional systems (see, for example, Refs. [9–14]).

Hence a promising approach for a first-principles description of orbital and multipolar ordering phenomena consists in using the DFT+DMFT method to evaluate an effective low-energy Hamiltonian describing intersite interactions between

localized shells. Such Hamiltonians can then be solved by a variety of methods developed for Heisenberg and similar models in order to predict the ordered phase as a function of external parameters like pressure or temperature.

Several such techniques have been proposed [15–21] for evaluating low-energy spin Hamiltonians in conjunction with standard DFT methods. They were subsequently also extended to calculations, for example, of the magnetic crystalline anisotropy [22] and Dzyaloshinskii-Moriya interactions [23]. Generally, in those approaches effective exchange interactions are extracted by considering a first-order response of the grand potential upon a simultaneous change of magnetic configurations of two neighboring sites. In particular, in those approaches that have been to date generalized for correlated systems (Refs. [24–26]), one computes the variation of the grand potential of a magnetically ordered state upon simultaneous small tilting of two neighboring spins.

The technique proposed in this work in order to calculate intersite dipolar and multipolar interactions is similar in spirit to those methods. However, in contrast to them, we will calculate the variation of the DFT+DMFT grand potential of the *paramagnetic* (symmetry-unbroken) phase upon simultaneous small change of the atomic configurations of correlated shells of two neighboring sites. Hence one can derive intersite interactions directly from the high-temperature paramagnetic state, which is typically most readily accessible for DFT+DMFT. The approach is currently formulated using the atomic (Hubbard-I) [27] approximation for the DMFT local self-energy. It is fast and, in principle, able to calculate all terms of the low-energy Hamiltonian, including non-Ising spin-spin, spin-orbital, and multipolar interactions. The formulation on the basis of Hubbard-I entails, however, certain limitations. In particular, the present approach is suitable for localized systems like TM oxides and local-moment lanthanide compounds and cannot be applied to metals.

As a first application of this technique to real materials, we study the spin-orbital ordering in the cubic phase of the Mott insulator KCrF_3 . In this compound, the $3d$ shell of the

*leonid.pourovskii@polytechnique.edu

Cr^{2+} ion is in the high-spin $t_{2g}^3 e_g^1$ configuration with the spin of a single e_g electron aligned to that of the half-filled t_{2g} subshell by the Hund's rule coupling, similarly to undoped peroxide manganese LaMnO_3 . KCrF_3 adopts the cubic peroxide structure at high temperatures. At $T_{\text{OO}} \approx 973$ K, it undergoes a first-order orbital-ordering transition accompanied by a tetragonal distortion (space group $I4/mcm$) [28]. Another structural transition to a low-temperature monoclinic phase (space group $I112/m$) due to tilting of the CrF_6 octahedra is observed at $T \approx 250$ K [29]. Finally, a transition into an incommensurate layered antiferromagnetic (AFM) phase with the ordering vector $(1/2 \pm \delta, 1/2 \pm \delta, 0)$ in the monoclinic cell is taken place at $T_N \approx 80$ K [30]. Below 46 K, the AFM order becomes a fully commensurate A-type one with $\delta \rightarrow 0$, a spin canting is detected below 9.5 K leading to formation of a small ferromagnetic moment [30].

As in other Jahn-Teller systems, it is important to disentangle the lattice and purely electronic superexchange contributions into the spin-orbital ordering in KCrF_3 to understand their relative importance. Previously the orbital ordering in the undistorted cubic structure has been studied theoretically within DFT+DMFT [31] and DFT+ U [32,33] approaches. In particular, the authors of Ref. [31] derived an effective DMFT impurity problem for the Cr e_g subshell with a simplified treatment of its interactions with the t_{2g} spin, which was subsequently solved by a quantum Monte Carlo (QMC) method. They obtained a substantially underestimated value $T_{\text{OO}} \approx 400$ K when only the supexchange contribution was taken into account.

Here we compute all relevant superexchange interactions for the cubic phase of KCrF_3 and then solve the resulting effective spin-orbital Hamiltonian within the mean-field approximation obtaining orbital and magnetic ordering temperatures and the corresponding phases. We find an underestimated value of T_{OO} in agreement with Ref. [31], in contrast, the calculated value for T_N and the predicted A type of the AFM order agree with those experimentally observed in KCrF_3 . We show that the onset of the AFM phase produces a feedback effect on the orbital arrangement leading to a loss of the perfect antiferro-orbital order even in the absence of lattice distortions.

The rest of paper is organized as follows: the method is derived in Sec. II. It is subsequently tested and its limitations explored by applying it to one-band and two-band e_g Hubbard model on the simple-cubic lattice in Secs. III and IV, respectively. Finally, its application to KCrF_3 and the obtained results are presented in Sec. V.

II. METHOD

We start by deriving in Sec. II A the variation of the Hubbard-I self-energy with respect to a change of the atomic configuration of correlated shell. The derived expressions are then used in Sec. II B to calculate the variation of the DFT+DMFT grand potential upon simultaneous change of atomic configurations on two neighboring sites and, thus, to extract the corresponding intersite interactions between those configurations. Finally, in Sec. II C, we recast the obtained interactions into a more conventional dipolar and multipolar form. The full calculational procedure is shortly outlined in Sec. II D.

A. Local fluctuations within the Hubbard-I approximation

Let us first outline the main features of the Hubbard-I approximation (HIA) as applied to the DMFT quantum impurity problem. In this case, the HIA can be derived by a high-frequency expansion of the DMFT self-consistency condition (see, e.g., Ref. [34]) to the first order in $1/\omega$, leading to the following expression for the noninteracting level positions of the impurity:

$$\epsilon = -I\mu + \sum_{\mathbf{k}} P_{\mathbf{k}} H_{\text{KS}}^{\mathbf{k}} P_{\mathbf{k}}^{\dagger} - \Sigma_{\text{dc}} \quad (1)$$

where $H_{\text{KS}}^{\mathbf{k}}$ and $P_{\mathbf{k}}$ are the Kohn-Sham (KS) Hamiltonian and “projector” between the KS and correlated spaces for a given \mathbf{k} point in the Brillouin zone (BZ), respectively, Σ_{dc} is the double-counting correction for the self-energy, μ is the chemical potential, and I is the unit matrix. The DMFT bath Green's function \mathcal{G} within the HIA takes a very simple form

$$\mathcal{G}_0^{-1}(i\omega_n) = i\omega_n I - \epsilon, \quad (2)$$

where $\omega_n = \pi T(2n - 1)$ is the fermionic Matsubara frequency. Solving of the impurity problem is then reduced to the diagonalization of the effective atomic Hamiltonian $H_{\text{at}} = \sum_{ab} \epsilon_{ab} f_a^{\dagger} f_b + H_U$, where $f_a^{\dagger} (f_b)$ is the creation(annihilation) operator for the localized orbital labeled by relevant quantum numbers designated by $a(b)$, H_U is the on-site Coulomb repulsion.

The corresponding atomic Green's function then reads

$$G_{ab}^{\text{at}}(i\omega_n) = \sum_{\gamma\gamma'} \frac{\langle \gamma | f_a | \gamma' \rangle \langle \gamma' | f_b^{\dagger} | \gamma \rangle}{i\omega_n - E_{\gamma'} + E_{\gamma}} (X_{\gamma} + X_{\gamma'}), \quad (3)$$

where $|\gamma\rangle$ and $|\gamma'\rangle$ are eigenstates of the atomic Hamiltonian H_{at} , E_{γ} and $X_{\gamma} = \frac{e^{-\beta E_{\gamma}}}{Z}$ are the corresponding eigenenergies and Boltzmann weights, respectively, Z is the partition function, $\beta = \frac{1}{T}$ is the inverse temperature. The atomic self-energy can then be calculated through the Dyson equation:

$$\Sigma^{\text{at}}(i\omega_n) = [\mathcal{G}_0(i\omega_n)]^{-1} - [G^{\text{at}}(i\omega_n)]^{-1}. \quad (4)$$

In cases where the HIA is applicable and for reasonable temperatures the system is far from the intermediate-valence regime, hence, charge fluctuations can be safely neglected. Moreover, in localized systems, the most important fluctuations are expected to occur among quasidegenerate states belonging to the ground-state (GS) atomic multiplet. For example, for $4f$ shells this multiplet is defined by the occupancy as well as by the spin S , orbital L , and total J quantum numbers, in TM ions, it is rather defined by the occupancy, S , and crystal field. In solids the GS multiplet can be additionally split by smaller energy scales, like the crystal field in rare-earths and the spin-orbit coupling in TM ions. Hence, here we consider fluctuations only among the states belonging to GS multiplet. It is useful for the following to recast the atomic GF into a slightly more general form:

$$G^{\text{at}} = \text{Tr}[\hat{\rho} \hat{G}] + G_1^{\text{at}}, \quad (5)$$

where the first term comprises all contributions to G^{at} involving the states of the GS multiplet; those states will be in the following designated by capital Greek letters, for example, $|\Gamma\rangle$. The rest is collected in G_1^{at} . The density matrix

$\hat{\rho}$ (throughout Sec. II we use the hat, \hat{X} , for any matrix X in the basis of atomic states $|\Gamma\rangle$) of the GS multiplet in the symmetry-unbroken (paramagnetic) state is defined within the HIA by

$$\rho_{\Gamma\Gamma'} = \delta_{\Gamma\Gamma'} \frac{e^{-\beta E_\Gamma}}{Z}, \quad (6)$$

where $\delta_{\Gamma\Gamma'}$ is the Kronecker delta, and the corresponding element of the atomic GF matrix \hat{G} in the imaginary time domain reads $G_{ab}^{\Gamma\Gamma'}(\tau) = -\langle \Gamma | T [f_a(\tau) f_b^\dagger(0)] | \Gamma' \rangle$, where T is the time-ordering operator, $|\Gamma\rangle$ and $|\Gamma'\rangle$ are eigenstates of H_{at} belonging to the GS multiplet. By the Fourier transform one obtains, e.g., for the off-diagonal matrix elements of \hat{G} in the frequency space:

$$G_{ab}^{\Gamma\Gamma'}(i\omega_n) = \sum_{\lambda \in Q+1} \frac{1 + e^{-\Delta E_{\Gamma\lambda}\beta}}{i\omega_n - \Delta E_{\Gamma\lambda}} (F^a)_{\Gamma\lambda} (F^{b\dagger})_{\lambda\Gamma'} + \sum_{\lambda \in Q-1} \frac{1 + e^{-\Delta E_{\Gamma'\lambda}\beta}}{i\omega_n + \Delta E_{\Gamma'\lambda}} (F^{b\dagger})_{\Gamma\lambda} (F^a)_{\lambda\Gamma'}, \quad (7)$$

where $(F^{a(\dagger)})_{\Gamma\lambda} = \langle \Gamma | f_a^{(\dagger)} | \lambda \rangle$, $\Delta E_{\Gamma\lambda} = E_\lambda - E_\Gamma$ is the energy difference between the state $|\Gamma\rangle$ belonging to the GS multiplet with the occupancy Q and the excited state $|\lambda\rangle$. Similar, but simpler expressions can be obtained for the diagonal elements $G_{ab}^{\Gamma\Gamma}$.

Let us now consider the change of the atomic Green's function upon a small fluctuation of the density matrix $\hat{\rho}$ with respect to its symmetry-unbroken Hubbard-I form (6). We define the fluctuation for diagonal elements $\rho_{\Gamma\Gamma}$ as a diagonal $N \times N$ matrix $\delta\hat{\rho}^{\Gamma\Gamma}$ with the following elements:

$$\delta\rho_{\Lambda\Lambda}^{\Gamma\Gamma} = \left(\frac{N-1}{N} \delta_{\Lambda\Gamma} + \frac{1}{N} (\delta_{\Lambda\Gamma} - 1) \right) \epsilon, \quad (8)$$

where N is the degeneracy of the ground-state multiplet, ϵ is a small parameter. As one may easily see, the fluctuation (8) conserves the trace of $\hat{\rho}$ and induces a corresponding fluctuation of an angular momentum of the shell. For example, if in the symmetry-unbroken state the value of an angular momentum operator \hat{J} is zero, $\text{Tr}[\hat{\rho}\hat{J}] = 0$ and $\langle \Gamma | \hat{J} | \Gamma \rangle = J_\Gamma$, then the corresponding fluctuation of the moment is $\text{Tr}[\delta\hat{\rho}^{\Gamma\Gamma}\hat{J}] = \epsilon J_\Gamma$.

We also define the off-diagonal fluctuation of $\delta\hat{\rho}^{\Gamma\Gamma'}$ as an $N \times N$ matrix with a single none-zero element:

$$\delta\rho_{\Lambda\Lambda'}^{\Gamma\Gamma'} = \delta_{\Gamma\Lambda} \delta_{\Gamma'\Lambda'} \epsilon. \quad (9)$$

Using the definition (5) for the atomic GF one then obtains the following expression for the variational derivative of G_{at} over a fluctuation of the type (8) or (9):

$$\frac{\delta G_{\text{at}}}{\delta \hat{\rho}^{\Gamma\Gamma'}} = G^{\Gamma\Gamma} - \delta_{\Gamma\Gamma'} \frac{\text{Tr}[\hat{G}]}{N}. \quad (10)$$

The second term in (5), G_{I}^{at} , does not contribute to the variational derivative (10), because the weights X_γ of the states not belonging to the GS multiplet are not affected by fluctuations of the types (8) and (9). Those fluctuations only redistribute the weights within the GS multiplet and do not change Z .

The corresponding variational derivative of the atomic self-energy (4) reads

$$\frac{\delta \Sigma^{\text{at}}}{\delta \hat{\rho}^{\Gamma\Gamma'}} = [G^{\text{at}}]^{-1} \left(G^{\Gamma\Gamma} - \delta_{\Gamma\Gamma'} \frac{\text{Tr}[\hat{G}]}{N} \right) [G^{\text{at}}]^{-1}. \quad (11)$$

In the next section, we will make use of (11) to calculate the response of the DFT+DMFT grand potential upon small fluctuations of the density matrix (6) on two neighboring sites.

B. Response of the grand potential and effective intersite interactions

The DFT+DMFT grand potential [7,35,36] reads

$$\begin{aligned} \Omega[n(\mathbf{r}), G^{\text{loc}}, \Delta\Sigma, V_{\text{KS}}] &= -\frac{1}{\beta} \text{Tr} \ln \left[i\omega_n + \mu + \frac{\nabla^2}{2} - V_{\text{KS}} - \Delta\Sigma \right] - \text{Tr}[G^{\text{loc}} \Delta\Sigma] \\ &\quad + \sum_{\mathbf{R}} [\Phi^{\text{imp}}[G_{\mathbf{R}}^{\text{loc}}] - \Phi^{\text{dc}}[G_{\mathbf{R}}^{\text{loc}}]] + \Omega_r[n(\mathbf{r})] \\ &\equiv \Delta\Omega[G^{\text{loc}}, \Delta\Sigma, V_{\text{KS}}] + \Omega_r[n(\mathbf{r})], \end{aligned} \quad (12)$$

where $n(\mathbf{r})$ is the electronic density, V_{KS} is the Kohn-Sham one-electron potential, G^{loc} is the local GF, $\Delta\Sigma$ is the difference between the impurity self-energy Σ^{imp} and the double counting correction Σ^{dc} , $\Phi^{\text{imp}}[G_{\mathbf{R}}^{\text{loc}}]$ is the DMFT interaction energy functional for the site \mathbf{R} , $\Phi^{\text{dc}}[G_{\mathbf{R}}^{\text{loc}}]$ is the corresponding functional for the double-counting correction, and μ is the chemical potential. The last term $\Omega_r[n(\mathbf{r})]$ depends only on the electronic charge density $n(\mathbf{r})$, while all other terms collected in $\Delta\Omega[G^{\text{loc}}, \Delta\Sigma, V_{\text{KS}}]$ do not have an explicit dependence on $n(\mathbf{r})$. At the DMFT self-consistency, the local GF of the lattice problem G^{loc} should be equal to the impurity GF G^{imp} . Within the HIA, however, the full DMFT self-consistency is never achieved because the hybridization function is neglected in the impurity problem, $G^{\text{imp}} \equiv G^{\text{at}}$, but is included into the local GF of the lattice problem. Hence, within the HIA, one should always keep the distinction between G^{loc} and G^{imp} , where G^{imp} and Σ^{imp} calculated within the HIA in accordance with (3) and (4), respectively.

Let us now introduce the basis of Kohn-Sham eigenstates $\{\Psi_{\mathbf{k}\nu}\}$, where ν labels Kohn-Sham bands. The corresponding real-space (Wannier) basis functions are defined by $\Psi_{\mathbf{R}\nu}(\mathbf{r} - \mathbf{R}) = \frac{V}{(2\pi)^3} \int_{\text{BZ}} d\mathbf{k} e^{-i\mathbf{k}\mathbf{R}} \Psi_{\mathbf{k}\nu}(\mathbf{r})$, where V is the unit cell volume.¹ We also introduce a real-space basis of (localized) Wannier orbitals representing correlated states, $\{w_{\mathbf{R}a}\}$, where a labels orbitals at the correlated shell \mathbf{R} , as well as corresponding projectors between the KS and correlated subspaces, $P_{a\nu}^{\mathbf{R}\mathbf{R}'} = \langle w_{\mathbf{R}a} | \Psi_{\mathbf{R}'\nu} \rangle$. Using the real-space bases $\{\Psi_{\mathbf{R}\nu}\}$ and $\{w_{\mathbf{R}a}\}$ and within the HIA, one may rewrite $\Delta\Omega$

¹The Wannier transformation is gauge-invariant with respect to a unitary transformation of $\{\Psi_{\mathbf{k}\nu}\}$. For the present derivation, it is not important, hence, we assume that the corresponding unitary matrix is equal to unity.

as follows:

$$\begin{aligned} \Delta\Omega[G^{\text{loc}}, \Delta\Sigma, V_{\text{KS}}] = & -\frac{1}{\beta} \text{Tr} \ln[\mathcal{M}_n] - \sum_{\mathbf{R}} \text{Tr}[G_{\mathbf{R}}^{\text{loc}} \Sigma_{\mathbf{R}}^{\text{at}}] \\ & + \sum_{\mathbf{R}} \text{Tr}[G_{\mathbf{R}}^{\text{loc}} \Sigma_{\mathbf{R}}^{\text{dc}}] \\ & + \sum_{\mathbf{R}} [\Phi^{\text{at}}[G_{\mathbf{R}}^{\text{loc}}] - \Phi^{\text{dc}}[G_{\mathbf{R}}^{\text{loc}}]], \quad (13) \end{aligned}$$

where elements of the real-space matrix \mathcal{M}_n read

$$\begin{aligned} \mathcal{M}_n^{\mathbf{R}\mathbf{R}'} = & (i\omega_n + \mu)I - H_{\text{KS}}^{\mathbf{R}\mathbf{R}'} \\ & - \sum_{\mathbf{R}''} P_{\mathbf{R}\mathbf{R}''}^{\dagger} (\Sigma_{\mathbf{R}''\mathbf{R}'}^{\text{at}}(i\omega_n) - \Sigma_{\mathbf{R}''\mathbf{R}'}^{\text{dc}}) P_{\mathbf{R}''\mathbf{R}'}, \quad (14) \end{aligned}$$

$H_{\text{KS}}^{\mathbf{R}\mathbf{R}'}$ and $\Sigma_{\mathbf{R}\mathbf{R}'}^{\text{at}}(i\omega_n)$ are matrices in the band and correlated orbitals' spaces, respectively, the matrix elements of the former are given by $[H_{\text{KS}}^{\mathbf{R}\mathbf{R}'}]_{\nu\nu'} = \langle \Psi_{\mathbf{R}\nu} | -\frac{\nabla^2}{2} + \hat{V}_{\text{KS}} | \Psi_{\mathbf{R}'\nu'} \rangle$.

We will now calculate the response of the grand potential (12) upon simultaneous fluctuations of atomic configurations of correlated shells on two *different* atomic sites, i.e., we evaluate $\frac{\delta^2 \Omega}{\delta \hat{\rho}^{\Gamma_1 \Gamma_2}(\mathbf{R}) \delta \hat{\rho}^{\Gamma_3 \Gamma_4}(\mathbf{R}')}$. First, in the usual ‘‘force theorem’’ spirit [19,37,38], one may neglect, to the first order in $\delta \hat{\rho}^{\Gamma_1 \Gamma_2}(\mathbf{R}) \delta \hat{\rho}^{\Gamma_3 \Gamma_4}(\mathbf{R}')$, the contribution due to the renormalization of the charge density, i.e., the contribution from $\Omega_r[n(\mathbf{r})]$. One may also notice that all terms in (13), apart from the first one, are site-diagonal and will not contribute to a variational derivative over configurations of two different sites. Hence the only nonzero contribution due to simultaneous fluctuations on two different sites \mathbf{R} and \mathbf{R}' is due to the first term in (13). \mathcal{M}_n dependence on the correlated shell configuration stems from that of the atomic self-energy Σ^{at} . The double-counting correction Σ^{dc} for a paramagnetic phase depends only on the total shell occupancy, which is not affected by the density-matrix variations (8) and (9). Performing the derivative $\frac{\delta^2 [-\frac{1}{\beta} \text{Tr} \ln[\mathcal{M}_n]]}{\delta \hat{\rho}^{\Gamma_1 \Gamma_2}(\mathbf{R}) \delta \hat{\rho}^{\Gamma_3 \Gamma_4}(\mathbf{R}')}$ and making use of the ‘‘folding’’ property of projector matrices, $\sum_{\mathbf{R}_1 \mathbf{R}_2} P_{\mathbf{R}\mathbf{R}_1} [\mathcal{M}_n^{-1}]_{\mathbf{R}_1 \mathbf{R}_2} [P_{\mathbf{R}_2 \mathbf{R}'}]^{\dagger} = G_{\mathbf{R}\mathbf{R}'}$, one obtains

$$\begin{aligned} \frac{\delta^2 \Omega}{\delta \hat{\rho}^{\Gamma_1 \Gamma_2}(\mathbf{R}) \delta \hat{\rho}^{\Gamma_3 \Gamma_4}(\mathbf{R}')} & \equiv \langle M_1 M_3 | V^{\mathbf{R}\mathbf{R}'} | M_2 M_4 \rangle \\ & = \frac{1}{\beta} \text{Tr} \left[G_{\mathbf{R}\mathbf{R}'} \frac{\delta \Sigma_{\mathbf{R}'}^{\text{at}}}{\delta \hat{\rho}^{\Gamma_3 \Gamma_4}} G_{\mathbf{R}'\mathbf{R}} \frac{\delta \Sigma_{\mathbf{R}}^{\text{at}}}{\delta \hat{\rho}^{\Gamma_1 \Gamma_2}} \right], \quad (15) \end{aligned}$$

where the derivative $\frac{\delta \Sigma_{\mathbf{R}}^{\text{at}}}{\delta \hat{\rho}^{\Gamma_1 \Gamma_2}}$ over an on-site fluctuation is given by Eq. (11), M_j is the relevant set of quantum numbers labeling the state Γ_j and the ‘‘intersite’’ GF $G_{\mathbf{R}\mathbf{R}'}$ can be calculated as a Fourier transform of the DMFT lattice GF in the reciprocal space:

$$\begin{aligned} G_{\mathbf{R}\mathbf{R}'}(i\omega_n) = & \frac{V}{(2\pi)^3} \int_{\text{BZ}} d\mathbf{k} e^{-i\mathbf{k}(\mathbf{R}'-\mathbf{R})} P_{\mathbf{k}} \\ & \times [i\omega_n + \mu - H_{\text{KS}}^{\mathbf{k}} - P_{\mathbf{k}}^{\dagger} \Delta \Sigma P_{\mathbf{k}}]^{-1} P_{\mathbf{k}}^{\dagger}. \quad (16) \end{aligned}$$

In Eq. (15), we identify $\frac{\delta^2 \Omega}{\delta \hat{\rho}^{\Gamma_1 \Gamma_2}(\mathbf{R}) \delta \hat{\rho}^{\Gamma_3 \Gamma_4}(\mathbf{R}')}$ with the corresponding intersite interaction of an effective low-energy

Hamiltonian of the system:

$$\hat{H}_{\text{eff}} = \sum_{\mathbf{R}, \Gamma} E_{\Gamma} \hat{\rho}_{\Gamma}^{\mathbf{R}} + \sum_{\substack{\mathbf{R}\mathbf{R}' \\ 1234}} \langle 13 | V^{\mathbf{R}\mathbf{R}'} | 24 \rangle \hat{\rho}_{12}^{\mathbf{R}} \hat{\rho}_{34}^{\mathbf{R}'}, \quad (17)$$

where $\hat{\rho}_{\Gamma}^{\mathbf{R}} = |\Gamma^{\mathbf{R}}\rangle \langle \Gamma^{\mathbf{R}}|$ is the corresponding projection (Hubbard) operator between the atomic states Γ and Γ_1 belonging to the ground-state multiplet of the site \mathbf{R} , E_{Γ} is the one-site (crystal-field) term, $\langle 13 | V^{\mathbf{R}\mathbf{R}'} | 24 \rangle$ is the intersite interaction between the corresponding Hubbard operators on the sites \mathbf{R} and \mathbf{R}' (here the label Γ is suppressed and the short-hand notation $1 \equiv M_1$ is used).

The identification of the corresponding intersite interaction in \hat{H}_{eff} with (15) can be justified using, e.g., the approach of Refs. [36,39,40]. Using this approach, one may write a (Legendre-transformed) grand potential corresponding to (17) for a set of preassigned on-site occupancy matrices $\{\rho^{\mathbf{R}}\}$ as $\Omega_{LT}[\rho] = \Omega_0[\rho] + \sum_{\mathbf{R}\mathbf{R}'} \langle 13 | V^{\mathbf{R}\mathbf{R}'} | 24 \rangle \hat{\rho}_{12}^{\mathbf{R}} \hat{\rho}_{34}^{\mathbf{R}'}$ +

$\Omega_{\text{corr}} = \Omega_{MF} + \Omega_{\text{corr}}$, where Ω_{MF} and Ω_{corr} is the mean-field and beyond-mean-field contributions, respectively, $\Omega_0[\rho]$ is the one-site term. Setting the density matrices $\hat{\rho}^{\mathbf{R}}$ to their mean-field values in the symmetry-unbroken state and computing the variational derivative of Ω_{MF} over $\delta \hat{\rho}_{12}^{\mathbf{R}} \delta \hat{\rho}_{34}^{\mathbf{R}'}$ one obtains $\langle 13 | V^{\mathbf{R}\mathbf{R}'} | 24 \rangle$. Hence, one identifies the derivative (15) of the dynamical *mean-field* grand potential (12) as the corresponding intersite interaction in (17). Of course, the usefulness of those interactions depends on whether the effective Hamiltonian (17) indeed describes the low-energy physics of (12). This should be the case for strongly-correlated local-moment systems, e.g., for rare-earth intermetallics above their Kondo temperature or for Mott insulators.

C. Multipolar formalism

The intersite interactions between atomic states $|\Gamma\rangle$ calculated in accordance with (15) can be used directly, e.g., in an effective Hamiltonian of the type (17). This Hamiltonian is written in terms of low-energy interactions between the on-site Hubbard operators defined above describing transitions between atomic states belonging to the ground-state multiplet.

However, the standard dipolar and multipolar tensor operators are, in fact, linear combinations of those Hubbard operators with coefficients written in terms of the corresponding Wigner $3j$ symbols [4,41]. Hence, instead of working directly with the Hubbard-operator form (17), one may recast this Hamiltonian to describe interactions between dipole and multipole (quadrupole, octopole, etc.) operators acting on neighboring sites. The low-energy Hamiltonian in this form is more standard (one may recall, for example, the spin Heisenberg and spin-orbit Kugel-Khomskii Hamiltonians) and also more compact when additional symmetries are present. Moreover, it is written in terms of operators which expectation values, i.e., dipole and multipole moments, are directly measured experimentally. In this section, we derive a transformation relating intersite interactions in the density-matrix (17) and more conventional dipolar-multipolar Hamiltonians.

We start by briefly summarizing properties of tensor operators. The spherical tensor operators in the basis of

angular-momentum eigenstates $|JM\rangle$ are standardly defined as follows [4,41]:

$$\begin{aligned}\hat{T}_{KQ}(J) &= \sum_{MM'} T_{KQ}^{MM'}(J) |JM\rangle \langle JM'| \\ &= \sum_{MM'} T_{KQ}^{MM'}(J) \hat{\rho}_{MM'},\end{aligned}\quad (18)$$

where K and Q label the multipole rank and component, respectively, $2J + 1$ states $|JM\rangle$ belong to the ground-state multiplet specified by the angular-momentum quantum number J , $M = -J, \dots, J$, $\hat{\rho}_{MM'} \equiv |JM\rangle \langle JM'|$ is the Hubbard operator acting within the ground-state multiplet, the coefficients $T_{KQ}^{MM'}(J)$ read

$$T_{KQ}^{MM'}(J) = (-1)^{J-M} (2K+1)^{1/2} \begin{pmatrix} J & J & K \\ M' & -M & Q \end{pmatrix}. \quad (19)$$

The set of $(2J+1)^2$ operators $\hat{T}_{KQ}(J)$ with $K = 0, 1, \dots, 2J$, (i.e., monopole, dipole, etc. operators) and $Q = -K, \dots, K$ is complete in the subspace spanned by the $|JM\rangle$ states and any operator acting in this subspace can be represented as a linear superposition of $\hat{T}_{KQ}(J)$. Other properties of those operators are discussed, e.g., in Refs. [4,41]. In particular, one may notice that the tensor operators (18) cannot represent observables as they are not self-adjoint [41], $\hat{T}_{KQ}^\dagger = (-1)^{-Q} \hat{T}_{K-Q}$, for $Q \neq 0$. However, the self-adjoint linear combinations of \hat{T}_{KQ} can be formed similarly to the real spherical harmonics:

$$\hat{O}_{KQ}(J) = \sum_{MM'} O_{KQ}^{MM'}(J) \hat{\rho}_{MM'}, \quad (20)$$

where

$$\begin{aligned}O_{KQ}^{MM'}(J) &= \frac{1}{\sqrt{2}} [(-1)^Q T_{KQ}^{MM'}(J) + T_{K-Q}^{MM'}(J)], \\ O_{KQ}^{MM'}(J) &= \frac{i}{\sqrt{2}} [T_{K-Q}^{MM'}(J) - (-1)^Q T_{KQ}^{MM'}(J)],\end{aligned}\quad (21)$$

for $Q > 0$ and $Q < 0$, respectively. For example, for the dipole, $K = 1$, the components Q equal to $-1, 0$, and 1 transform under rotations as Cartesian y, z , and x , respectively, similarly to the corresponding real spherical harmonics.

One may introduce intersite interaction between the tensor operators (20) acting at sites \mathbf{R} and \mathbf{R}' as $\sum_{KK'} V_{KK'}^{QQ'}(\mathbf{R}\mathbf{R}') \hat{O}_{KQ}(\mathbf{R}) \hat{O}_{K'Q'}(\mathbf{R}')$, where the tensor operators of the rank $K(K')$ and for the component $Q(Q')$ are defined for the ground-state multiplet J of the corresponding atomic shell $\mathbf{R}(\mathbf{R}')$, respectively. The label J in $\hat{O}_{KQ}(\mathbf{R})$ is suppressed here to simplify the notation. It is easy to show that $\sum_{KK'} V_{KK'}^{QQ'}(\mathbf{R}\mathbf{R}') O_{KQ}^{M_1 M_2} O_{K'Q'}^{M_3 M_4}$ is equal to the intersite interaction $\langle M_1 M_3 | V^{\mathbf{R}\mathbf{R}'} | M_2 M_4 \rangle$ defined in (15) and (17).

By making use of the orthogonality relations of the $3j$ symbols, one may also show that $\sum_{MM'} O_{KQ}^{MM'}(J) O_{K'Q'}^{M'M}(J) = \delta_{KK'} \delta_{QQ'}$. Then by multiplying the intersite interactions (15) by $O_{KQ}^{M_2 M_1}(J)$ and $O_{K'Q'}^{M_4 M_3}(J)$ and summing over the quantum

numbers M , one obtains

$$\sum_{\substack{M_1 M_2 \\ M_3 M_4}} \langle M_1 M_3 | V^{\mathbf{R}\mathbf{R}'} | M_2 M_4 \rangle O_{KQ}^{M_2 M_1}(J) O_{K'Q'}^{M_4 M_3}(J) = V_{KK'}^{QQ'}(\mathbf{R}\mathbf{R}'). \quad (22)$$

Using (22), one may transform the intersite interactions from the atomic-level, Eq. (15), to multipolar form.²

In many cases, intersite interactions and corresponding ordering temperatures come out to be much smaller than the crystal field (CF) splitting within the ground-state multiplet J . In this case, one may restrict oneself to determining intersite interactions between the states belonging to the lowest CF level. For example, one may represent the state of an e_g TM ion by a product of the ordinary spin s and pseudospin τ quantum numbers, with the opposite directions of the pseudo-spin corresponding to the $3z^2 - r^2$ and $x^2 - y^2$ orbitals, respectively. This representation is widely used for TM oxides [1]. In this case one may introduce another type of tensor operators, the double tensor, which is a direct product of two spherical tensors for $J = 1/2$ and can be written using (21) as follows:

$$\begin{aligned}\hat{O}_{\Lambda\Sigma}^{\mu\nu} &= \sum_{\tau\tau'} \sum_{ss'} O_{\Lambda\mu}^{\tau\tau'}(1/2) O_{\Sigma\nu}^{ss'}(1/2) |\tau s\rangle \langle \tau' s'| \\ &= \sum_{\tau\tau'} \sum_{ss'} O_{\Lambda\Sigma}^{\mu\nu}(\tau s; \tau' s') \hat{\rho}_{\tau s; \tau' s'},\end{aligned}\quad (23)$$

where we again use the corresponding Hubbard operator $\hat{\rho}_{\tau s; \tau' s'} \equiv |\tau s\rangle \langle \tau' s'|$. The subscripts $\Lambda\Sigma$ and superscripts $\mu\nu$ in $\hat{O}_{\Lambda\Sigma}^{\mu\nu}$ are the ranks and components, respectively, of the single tensors forming the direct product. Then, for example, in the ‘‘double’’ spin-orbital space $\hat{O}_{01}^{0p} = \hat{s}_p$ and $\hat{O}_{10}^{p0} = \hat{\tau}_p$ will designate the spin and orbital dipole tensors, respectively, with $p = x, y$, or z . Analogously, spin-orbital combined tensors can be also introduced for the case of KCrF_3 or other compounds with the high-spin $t_{2g}^3 e_g^1$ shell, the only difference is that the $J = 2$ tensor $\hat{O}_{\Sigma\nu}(2)$ is used in this case to describe the spin.

Similarly to (22) the corresponding interactions read

$$\sum_{1234} \langle 13 | V^{\mathbf{R}\mathbf{R}'} | 24 \rangle O_{\Lambda\Sigma}^{\mu\nu}(2; 1) O_{\Lambda'\Sigma'}^{\mu'\nu'}(4; 3) = V_{\Lambda\Sigma; \Lambda'\Sigma'}^{\mu\nu; \mu'\nu'}(\mathbf{R}\mathbf{R}'), \quad (24)$$

where the short-hand notation $1 \equiv \{\tau_1 s_1\}$ is used. Finally, instead of using the tensors as defined in Eqs. (20) and (23), one may wish to write the interactions in terms of more conventional spin operators for the dipole case and the unit matrix for the monopole one, respectively, by renormalizing the intersite interactions as follows:

$$J_{\Lambda\Sigma; \Lambda'\Sigma'}^{\mu\nu; \mu'\nu'}(\mathbf{R}\mathbf{R}') = V_{\Lambda\Sigma; \Lambda'\Sigma'}^{\mu\nu; \mu'\nu'}(\mathbf{R}\mathbf{R}') c(\Lambda) c(\Sigma) c(\Lambda') c(\Sigma'), \quad (25)$$

²One may notice that off-diagonal interactions $\langle M_1 M_3 | V^{\mathbf{R}\mathbf{R}'} | M_2 M_4 \rangle$ with $M_1 \neq M_2$ and/or $M_3 \neq M_4$ may carry an arbitrary complex phase, which will then be passed to $V_{KK'}^{QQ'}(\mathbf{R}\mathbf{R}')$. To avoid this, we require that $|\Gamma\rangle \equiv |JM\rangle$ states used in (7) and (18) satisfy the usual phase convention with the matrix element of the ladder operator $\langle JM | J_+ | JM - 1 \rangle$ being a real positive number.

where the factor $c(\Lambda)$ is equal to $\frac{1}{\sqrt{2}}$ and $\sqrt{2}$ for Λ equal to 0 and 1, respectively [41].

We will label those interaction by τ and s for the dipole orbital and spin moments, respectively, as well as by q for the dipole-dipole (“quadrupole”) spin-orbital one. For example, $\hat{J}_{01;01}(\mathbf{R}\mathbf{R}') \equiv \hat{J}_{ss}(\mathbf{R}\mathbf{R}')$ is the spin-spin dipole-dipole interaction, $\hat{J}_{10;10}(\mathbf{R}\mathbf{R}') \equiv \hat{J}_{\tau\tau}(\mathbf{R}\mathbf{R}')$ is the orbital-orbital dipole-dipole one, $\hat{J}_{10;11}(\mathbf{R}\mathbf{R}') \equiv \hat{J}_{\tau q}(\mathbf{R}\mathbf{R}')$ is the orbital-(spin-orbital) dipole-quadrupole one and so on. Finally, for the case of one atom per unit cell, we may always make use of the translational invariance, hence, $\mathbf{R}\mathbf{R}'$ can be substituted with $\Delta\mathbf{R} = \mathbf{R}' - \mathbf{R}$.

D. Outline of calculation procedure

Let us summarize the sequence of steps for calculating intersite interactions using the method described above. First, one carries out full self-consistent DFT+DMFT calculations using the Hubbard-I approximation as the impurity solver. Second, one computes the atomic Green’s function matrix elements (7) and the variation derivative of the atomic self-energy (11) as well as the intersite DMFT Green’s function in the real space (16). Finally, the intersite interactions are computed in accordance with (15) and then transformed, if desired, into a suitable multipolar form using (22) or (24). The method is implemented numerically using the TRIQS library [42].

III. ONE-BAND HUBBARD MODEL

In this section, we benchmark the approach presented in Sec. II by applying it to a simple example of the one-band particle-hole symmetric Hubbard model on the 3d simple cubic lattice. The Hamiltonian of this model reads

$$\hat{H}_{1b} = \sum_{\mathbf{k}\sigma} \epsilon_{\mathbf{k}} f_{\mathbf{k}\sigma}^\dagger f_{\mathbf{k}\sigma} + U \sum_i \left(\hat{n}_{i\uparrow} - \frac{1}{2} \right) \left(\hat{n}_{i\downarrow} - \frac{1}{2} \right) \quad (26)$$

where \mathbf{k} belongs to the first Brillouin zone of the simple cubic lattice, $\hat{n}_{i\sigma} = f_{i\sigma}^\dagger f_{i\sigma}$ is the number operator for the site i and spin σ . For the simple cubic lattice with the nearest-neighbor hopping t , the band energy $\epsilon_{\mathbf{k}} = -2t(\cos k_x + \cos k_y + \cos k_z)$, where k_α are in units of the inverse lattice spacing $1/a$. Applying the Hubbard-I approximation in the framework of DMFT to \hat{H}_{1b} as described in Sec. II A and under the condition of $T \ll U$, one obtains $G^{\text{at}}(i\omega_n) = (\frac{1/2}{i\omega_n + U/2} + \frac{1/2}{i\omega_n - U/2})$ and $\Sigma^{\text{at}}(i\omega_n) = \frac{U^2}{4i\omega_n}$ for the atomic GF (3) and self-energy (4), respectively. Then one may easily obtain intersite interactions of the effective low-energy model at $t \ll U$ analytically by computing the intersite GF using the Fourier transform (16) and the variational derivatives of the atomic self-energy using Eqs. (7) and (11), respectively, and then inserting the result in (15). For example, by inserting the nearest-neighbor intersite GF $G_{\mathbf{R}\mathbf{R}'\in NN}^{\sigma\sigma'}(i\omega_n) = -\frac{\delta_{\sigma\sigma'} t}{(i\omega_n - \frac{U^2}{4i\omega_n})^2}$ and the “off-diagonal” derivative of the atomic

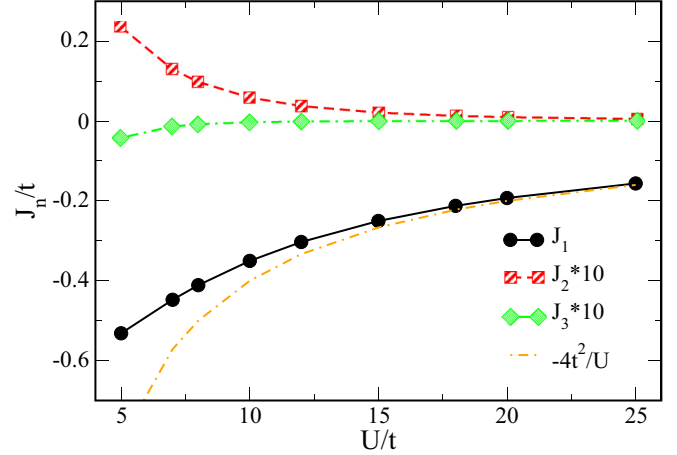


FIG. 1. Calculated intersite interactions J_n for the first three coordinational shells. The values of J_2 and J_3 are multiplied by 10. The dash-dotted line is the $-4t^2/U$ asymptote.

self-energy ($\frac{\delta \Sigma^{\text{at}}}{\delta \hat{\rho}^{\uparrow\downarrow}}$ is the same expression transposed)

$$\frac{\delta \Sigma^{\text{at}}}{\delta \hat{\rho}^{\uparrow\downarrow}}(i\omega_n) = \left(i\omega_n - \frac{U^2}{4i\omega_n} \right)^2 \times \begin{pmatrix} 0 & \frac{U}{\omega_n^2 + U^2/4} \\ 0 & 0 \end{pmatrix} \quad (27)$$

into (15) and carrying out the summation over Matsubara frequencies and spins, one obtains $\frac{2t^2}{U}$ for the nearest-neighbor spin-off-diagonal matrix element $\langle \uparrow\downarrow | V(\mathbf{d}) | \downarrow\uparrow \rangle$ (where the lattice vector $\mathbf{d} = \mathbf{R}' - \mathbf{R}$ connects nearest neighbors). This is indeed the correct value for this matrix element of the low-energy model for \hat{H}_{1b} at $t \ll U$, which is well known to be the spin-1/2 Heisenberg model

$$\hat{H}_H = - \sum_{ij} J_n \hat{s}_i \hat{s}_j, \quad (28)$$

where the interaction is isotropic and depends only on the distance $|\mathbf{R}_i - \mathbf{R}_j|$, i.e., on the coordination shell n . In the lowest order in t/U , only the nearest-neighbor antiferromagnetic interaction $J_1 = -\frac{4t^2}{U}$ survives in \hat{H}_H .

We have calculated numerically all matrix elements of (28) for several first coordinational shells as a function of U/t using (15) and then applied the transformation (22) to obtain the corresponding intersite interactions between the dipole tensor operators for spin 1/2. As expected, those interactions come out to be isotropic and direction-independent, $V_{11}^{xx}(\mathbf{d}) = V_{11}^{yy}(\mathbf{d}) = V_{11}^{zz}(\mathbf{d}) = V_n$. Finally, the tensor interactions V_n are renormalized, $J_n = 2V_n$ (cf. eq. 25), for the standard angular-momentum-operator form (28) of the Heisenberg Hamiltonian \hat{H}_H . The resulting J_n are plotted in Fig. 1 as a function of U/t . One sees that J_1 deviates stronger from the $-4t^2/U$ asymptote with increasing t and, simultaneously, the second and third coordinational sphere interactions increase though they still remain quite insignificant compared to J_1 .

The calculated interactions J_n have been used to evaluate the value of Néel temperature T_N for the model (26) within the mean-field approximation. The obtained values are compared

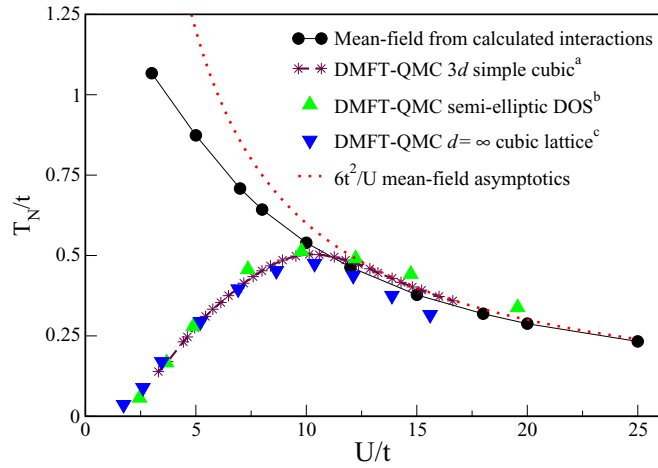


FIG. 2. Calculated values for the mean-field Néel temperature T_N compared with those obtained within QMC from (a) Ref. [10], (b) Ref. [43], and (c) Ref. [44] as well as with the large- U asymptote $T_N = \frac{6t^2}{U}$.

in Fig. 2 to T_N calculated within single-site DMFT using numerically exact quantum Monte Carlo (QMC) techniques [10,43,44]. The agreement with these numerically exact T_N is good for $U > 10t$. We note that within the dynamical mean-field theory, Heisenberg J_n not only define the transition temperature T_N but also directly impact the spectral properties of the Néel phase. In fact, J_n determine the spin-polaron peak structure within the Hubbard bands [45,46], which can be in some cases detected in real Mott insulators [46]. Hence one may suggest that the present approach can be possibly used to provide parameters for $t - J$ -like models aimed at investigating those phenomena.

For $U < 10t$, the present approach deviates significantly from the exact mean-field values, though less strongly than the simplest large- U asymptote. The value of $U \approx 10t$ at which the maximum of exact mean-field T_N is reached is very close to the critical value of U for the metal-insulator transition in the paramagnetic phase [47]. Hence one concludes that the present approach is reliable in the Mott-insulating regime.

IV. e_g -ORBITAL HUBBARD MODEL

Here we apply the method of Sec. II to a more complex model system, a two-band Hubbard model on the 3d simple cubic lattice, given by

$$\hat{H}_{2b} = \sum_{\substack{\langle ij \rangle \\ ab\sigma}} t_{ij}^{ab} f_{i\alpha\sigma}^\dagger f_{j\beta\sigma} + \hat{H}_{\text{int}}, \quad (29)$$

where $\langle ij \rangle$ runs over nearest-neighbor bonds, a and b label orbitals, t_{ij}^{ab} is the corresponding element of the hopping matrix, and \hat{H}_{int} is the on-site interaction term. We assume the orbitals to belong to the e_g representation of the cubic group for $l = 2$, $a \equiv 3z^2 - r^2$, and $b \equiv x^2 - y^2$, and employ the corresponding relations between the nearest-neighbor hopping integrals t_{ij}^{ab} , in which case the Fourier-transformed hopping

matrix reads

$$t(\mathbf{k}) = \begin{pmatrix} -\frac{1}{2}(\cos k_x + \cos k_y) - 2 \cos k_z & \frac{\sqrt{3}}{2}(\cos k_x - \cos k_y) \\ \frac{\sqrt{3}}{2}(\cos k_x - \cos k_y) & -\frac{3}{2}(\cos k_x + \cos k_y) \end{pmatrix} t \quad (30)$$

where t is the hopping between two $3z^2 - r^2$ orbitals for $\langle ij \rangle$ along the \hat{z} axis. By diagonalizing (30) one obtains e_g band dispersions with the total bandwidth $W = 6t$.

The interaction term H_{int} invariant over the cubic group symmetries reads (see, e.g., Refs. [48,49])

$$\begin{aligned} \hat{H}_{\text{int}} = & U \sum_{i,\alpha=a,b} \hat{n}_{i\alpha\uparrow} \hat{n}_{i\alpha\downarrow} + (U - 2J_H) \sum_{i,\alpha \neq \beta} \hat{n}_{i\alpha\uparrow} \hat{n}_{i\beta\downarrow} \\ & + (U - 3J_H) \sum_{i\sigma} \hat{n}_{i\sigma} \hat{n}_{i\bar{\sigma}} \\ & + J_H \sum_{i,\alpha \neq \beta} (f_{i\alpha\uparrow}^\dagger f_{i\alpha\downarrow}^\dagger f_{i\beta\downarrow} f_{i\beta\uparrow} - f_{i\alpha\uparrow}^\dagger f_{i\alpha\downarrow} f_{i\beta\downarrow}^\dagger f_{i\beta\uparrow}), \end{aligned} \quad (31)$$

where U and J_H are the Coulomb and Hund's rule interactions, respectively.

We study the case of one-quarter filling, $Q = 1$, for which the model (29) is relevant for a number of transition-metal compounds, for example, potassium copper fluorite KCuF_3 [1,48,50] and rare-earth nickelates RNiO_3 [51–53]. Essentially the same model was studied within DMFT in various parameter regimes to understand the behavior of nickelate-based heterostructures [54–56]. The magnitude of superexchange antiferromagnetic coupling is believed to be a crucial parameter controlling the physics of those heterostructures [54,57].

We first carried out DMFT calculations employing the HIA with J_H set either to 0 or to $0.5W$ and U being in the range from $5W$ to $15W$. The lower limit of U is chosen to be above the critical value $U_c = aW + 3J$ (where the prefactor a lies in the range from 1.5 to 2.5 depending on the lattice type under consideration) for the Mott transition in the two-band Hubbard model at quarter filling [53,58,59]. Then the superexchange intersite interactions at the first coordination shell between four one-electron states $|3z^2 - r^2, \uparrow\rangle$, $|3z^2 - r^2, \downarrow\rangle$, $|x^2 - y^2, \uparrow\rangle$, and $|x^2 - y^2, \downarrow\rangle$ were computed in accordance with (15). Finally, we employed Eqs. (24) and (25) to recast them into the standard Kugel-Khomskii [1] form of interacting spin-1/2 operators \hat{s} and $\hat{\tau}$ representing spin and orbital degrees of freedom, respectively ($\tau = 1/2$ and $\tau = -1/2$ designate occupied $x^2 - y^2$ and $3z^2 - r^2$, respectively). The resulting effective Hamiltonian for the [001] bond, $\langle ij \rangle || \hat{z}$, reads

$$\begin{aligned} \hat{H}_{\text{eff}}^{[001]} = & J_{ss} \sum_{\alpha} \hat{s}_{i\alpha} \hat{s}_{j\alpha} + J_{\tau\tau} \hat{\tau}_{iz} \hat{\tau}_{jz} + J_{qq} \sum_{\alpha} (\hat{s}_{i\alpha} \hat{\tau}_{iz})(\hat{s}_{j\alpha} \hat{\tau}_{jz}) \\ & + J_{sq} \sum_{\alpha} [\hat{s}_{i\alpha} (\hat{s}_{j\alpha} \hat{\tau}_{jz}) + (\hat{s}_{i\alpha} \hat{\tau}_{iz}) \hat{s}_{j\alpha}], \end{aligned} \quad (32)$$

where J_{ss} , $J_{\tau\tau}$, J_{sq} , and J_{qq} are the spin-spin, orbital-orbital, spin-(spin-orbital), and (spin-orbital)-(spin-orbital) interactions defined in Sec. II C, respectively, α runs over x , y , and z . As expected, the calculated effective Hamiltonians for the [100] and [010] bonds are related by the cubic symmetry to $\hat{H}_{\text{eff}}^{[001]}$ and can be obtained from it by the corresponding

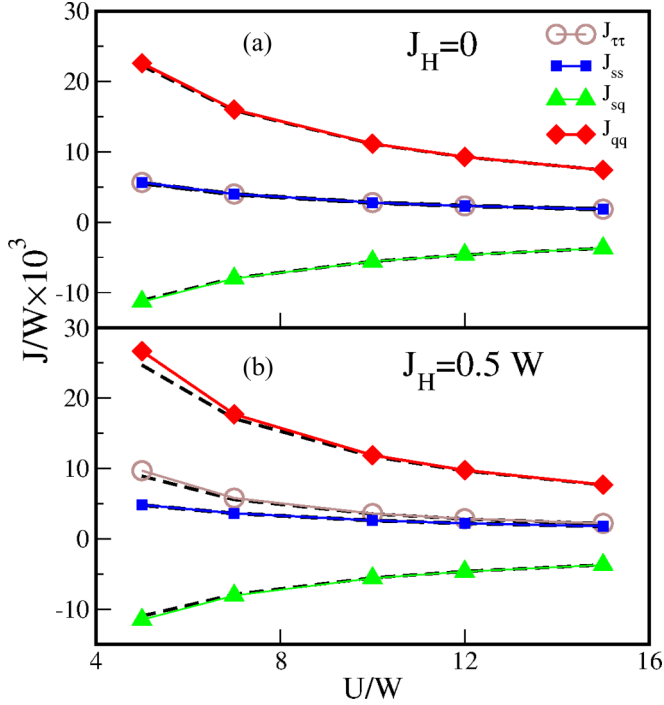


FIG. 3. Calculated superexchange intersite interactions for the e_g Hubbard model with (a) the Hund's rule coupling $J_H = 0$ and (b) $J_H = 0.5W$. The black dashed lines are the values obtained from analytical formulas (33).

rotation in the $\hat{\tau}$ space, i. e., by substituting $\hat{\tau}_z$ in (32) with $-\frac{1}{2}\hat{\tau}_z + \frac{\sqrt{3}}{2}\hat{\tau}_x$ and $-\frac{1}{2}\hat{\tau}_z - \frac{\sqrt{3}}{2}\hat{\tau}_x$, respectively.

The calculated values of J_{ss} , $J_{\tau\tau}$, J_{sq} , and J_{qq} versus U are displayed in Fig. 3 together with the corresponding values of those superexchange interactions obtained from the analytical expressions derived in Refs. [48,50]:

$$\begin{aligned} J_{ss} &= J(1 - \eta); & J_{\tau\tau} &= J(1 + 2\eta); \\ J_{sq} &= -J(2 - \eta); & J_{qq} &= 4J, \end{aligned} \quad (33)$$

where $J = \frac{t^2}{\tilde{U}}$, $\eta = \frac{2J_H}{\tilde{U}}$ with $\tilde{U} = U - J_H$ being the average Coulomb repulsion between e_g electrons with opposite spins. One may note a perfect agreement between the calculated and analytical values in Fig. 3(a) for the case $J_H = 0$, for which Eq. (33) reduce to $J_{ss} = J_{\tau\tau} = -J_{sq}/2 = J_{qq}/4 = \frac{t^2}{\tilde{U}}$. In the case of $J_H = 0.5W$ [Fig. 3(b)], there are small discrepancies between the present approach and the analytical formulas (33) at low values of U . This is apparently due to the fact that the formulas (33) were derived [48] by the first-order expansion in η and become less accurate with increasing J_H/U .

V. SPIN AND ORBITAL ORDERING IN KCrF_3

In this section, we calculate *ab initio* superexchange interactions for the cubic phase of KCrF_3 and then employ the resulting effective Hamiltonian to compute ordered phases and transition temperatures within the mean-field approximation. First, we carried out DFT+DMFT calculations of KCrF_3 using the linearized augmented plane-wave (LAPW) band structure method as implemented in the WIEN2K [60] code in conjunction with the DMFT and HIA implementations

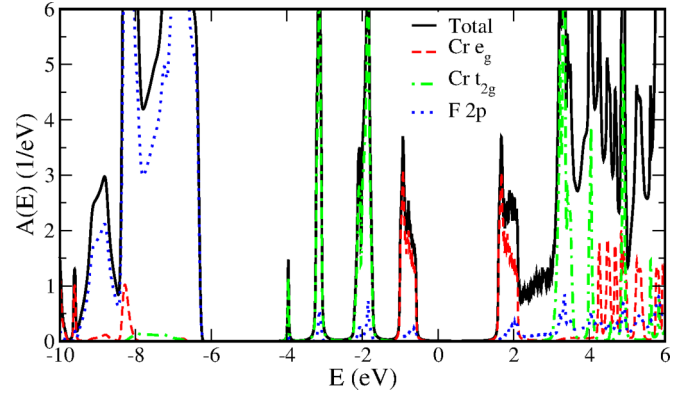


FIG. 4. The total and projected spectral functions of KCrF_3 calculated by the DFT+DMFT method within the Hubbard-I approximation using $U = 3.75$ eV.

provided by the TRIQS library [42,61]. The Wannier orbitals representing correlated Cr 3d states were constructed using the projective approach of Ref. [62] from the Kohn-Sham (KS) states in the window $[-2.7 : 2.7]$ eV around the Fermi level, this window encloses both e_g and t_{2g} -like KS bands. The self-consistency over the charge density in the DFT+DMFT calculations was implemented as described in Ref. [63], the spin-orbit coupling was neglected.

The rotationally invariant local Coulomb repulsion between all five Cr 3d orbitals was parametrized by the Slater integrals $F_0 = U = 3.75$ eV, as well as $F_2 = 6.44$ eV and $F_4 = 0.625F_6 = 4.025$ eV corresponding to the Hund's rule coupling $J_H = 0.75$ eV. Those values of $F_0 = U = 3.75$ and $J_H = 0.75$ eV were computed for KCrF_3 in Ref. [31] using a constrained-LDA technique. We also performed calculations with $U = 5$ eV for the sake of comparison. We employed the fully-localized-limit form for the double counting correction term calculated with the nominal Cr 3d shell occupancy of 4, this choice was shown to be appropriate for the HIA [34].

KCrF_3 was calculated in its high-temperature cubic peroxide structure with the experimental [28] lattice parameter of 4.23 Å. We employed the atomic sphere radii of 2.5, 2.0, and 1.78 a.u. for K, Cr, and F, respectively. The Brillouin zone (BZ) integration was carried out using 4000 \mathbf{k} -points in the full BZ, test calculations showed that increasing further the density of the \mathbf{k} -mesh had a negligible effect on the values of superexchange interactions.

Our DFT+DMFT calculations within HIA predict KCrF_3 to be a Mott insulator. Its spectral function features a Mott-Hubbard gap of about 2 eV, with the gap edges formed by e_g -like bands, see Fig. 4. The high-spin $t_{2g}^3 e_g^1$ configuration with the total spin $S = 2$ is predicted to be the ground-state multiplet of the Cr 3d shell, as expected. Due to the orbital degeneracy of $3z^2 - r^2$ and $x^2 - y^2$ the total degeneracy of the ground-state multiplet is $2(2S + 1) = 10$.

Effective intersite interactions (15) between those ten states belonging to the ground-state multiplet were then calculated in accordance with the approach of Secs. II A and II B. Then we again made use of Eqs. (24) and (25) to recast them into the Kugel-Khomskii form.

The calculated interactions between second nearest neighbors and beyond are at least two orders of magnitude smaller

TABLE I. Calculated Cr-Cr nearest-neighbor interactions along the [001] direction, in meV.

U (eV)	J_{ss}	$J_{\tau\tau}$	$J_{\tau\tau}^{xy}$	J_{sq}	J_{qq}	J_{qq}^{xy}
3.75	0.94	37.3	1.71	-1.77	7.12	0.28
5	0.96	24.7	1.20	-1.43	4.93	0.21

then those between the nearest neighbors and were neglected. The calculated superexchange Hamiltonian between two nearest neighbors i and j along the [001] direction has the following form:

$$\begin{aligned}
 \hat{H}_{\text{eff}}^{[001]} = & J_{ss} \sum_{\alpha} \hat{s}_{i\alpha} \hat{s}_{j\alpha} + J_{\tau\tau}^{xy} \sum_{\beta} \hat{\tau}_{i\beta} \hat{\tau}_{j\beta} + J_{\tau\tau} \hat{\tau}_{iz} \hat{\tau}_{jz} \\
 & + J_{sq} \sum_{\alpha} [\hat{s}_{i\alpha} (\hat{s}_{j\alpha} \hat{\tau}_{jz}) + (\hat{s}_{i\alpha} \hat{\tau}_{iz}) \hat{s}_{j\alpha}] \\
 & + J_{qq}^{xy} \sum_{\alpha\beta} (\hat{s}_{i\alpha} \hat{\tau}_{i\beta}) (\hat{s}_{j\alpha} \hat{\tau}_{j\beta}) \\
 & + J_{qq} \sum_{\alpha} (\hat{s}_{i\alpha} \hat{\tau}_{iz}) (\hat{s}_{j\alpha} \hat{\tau}_{jz}), \quad (34)
 \end{aligned}$$

where α and β run over x, y, z and x, y , respectively. The spin operators $\hat{s}_{i\alpha}$ act in the $S = 2$ space of the total spin of the site i , the $\tau = 1/2$ and $\tau = -1/2$ quantum numbers designate the $t_{2g}^3[x^2 - y^2]$ and $t_{2g}^3[3z^2 - r^2]$ shell configurations, respectively. The meaning of J_{ss} , $J_{\tau\tau}$, J_{sq} , and J_{qq} is the same as in Eq. (32) of Sec. IV. Comparing (34) to (32) one notices the appearance of new $J_{\tau\tau}^{xy}$ and J_{qq}^{xy} terms. Because there is no interorbital hopping within the e_g subshell along the z axis those terms should be related to virtual hopping of t_{2g} electrons [hence, they are absent from the pure e_g model, Eq. (32)].³

In Table I, we list the values of the intersite interactions calculated with $U = 3.75$ and 5 eV. One sees that the orbital-orbital $J_{\tau\tau}$ and (spin-orbital)-(spin-orbital) J_{qq} interactions are the most significant ones, even if one takes into account the different lengths of $\tau = 1/2$ and $S = 2$ spins. These interactions exhibit a strong reduction upon increasing U and decreasing J_H/U , cf. (33). The (spin-orbital)-(spin) term J_{sq} is also significant. $J_{\tau\tau}^{xy}$ and J_{qq}^{xy} are more than one order of magnitude smaller than $J_{\tau\tau}$ and J_{qq} , respectively.

We have then solved the calculated nearest-neighbor superexchange Hamiltonian defined by Eq. (34) (the nearest-neighbor interactions along the [100] and [010] directions are obtained from (34) using rotations in the τ space as described in Sec. IV) within the mean-field approximation using MCPHASE package [64] obtaining the total and free energies as well as stable ordered phases as a function of temperature.

The calculated temperature dependence of the specific heat [see Fig. 5(a)] features two clear phase transitions at temperatures of 340 and 102 K. The high-temperature one is an orbital-ordering transition, the obtained antiferro-orbital

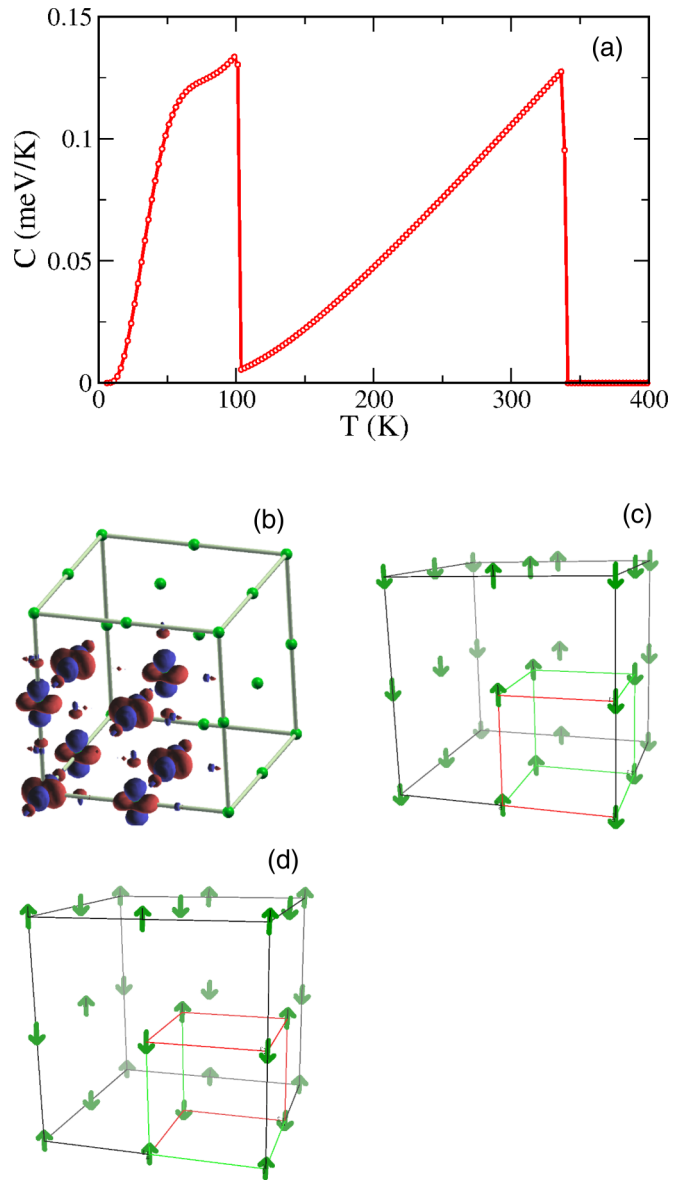


FIG. 5. (a) Specific heat (per formula unit) as a function of temperature obtained by solving the Hamiltonian (34) with the values of superexchange interactions calculated at $U = 3.75$ eV. (b) The G-type antiferro-orbital order obtained below $T_{OO} = 340$ K (plotted by XCRYSDEN [65], the real-space representation of the orbitals is generated with the help of the WPLOT [66] program). (c) The A-type antiferromagnetic phase, stable below $T_N = 102$ K, obtained with the interactions calculated with $U = 3.75$ eV. (d) The C-type antiferromagnetic phase obtained using the interactions calculated with $U = 5$ eV.

structure is displayed in Fig. 5(b). The occupied e_g states on two inequivalent sites [which are the nearest neighbors in the simple-cubic Cr sublattice, see Fig. 5(b)] in this structure can be written as

$$|\theta\rangle = \cos\theta|3z^2 - r^2\rangle + \sin\theta|x^2 - y^2\rangle, \quad (35)$$

$$|\theta_1\rangle = -\sin\theta_1|3z^2 - r^2\rangle + \cos\theta_1|x^2 - y^2\rangle, \quad (36)$$

³In fact, there is no symmetry reason for the interactions of $\hat{\tau}_{ix} \hat{\tau}_{jx}$ and $\hat{\tau}_{iy} \hat{\tau}_{jy}$ to be equal, however, we found them to be almost coinciding.

with $\theta = \theta_1$, hence, the obtained structure corresponds to a G-type antiferro-orbital order with the empty e_g orbital on the site one being occupied on the site two.⁴ The actual value of the angle θ is not defined by the Hamiltonian (34) in the absence of the spin ordering, experimentally it is fixed by the tetragonal lattice distortion and equal to 30° [28]. In fact, neglecting the lattice distortion leads to a strongly underestimated value of the temperature T_{OO} for the orbital ordering compared to experimental 973 K. The same result was obtained by Autieri *et al.* [31] using direct DMFT+QMC calculations and was shown to be due to the on-site crystal field splitting, the renormalization of hopping integrals due to the tetragonal (and subsequent monoclinic) distortion had an insignificant effect on T_{OO} .

The low-temperature transition at $T_N = 102$ K is due to ordering of Cr spins into the AFM A-type structure shown in Fig. 5(c). This structure consists of an antiferromagnetic stacking of ferromagnetically ordered xz layers, with each Cr site having four in-plane neighbors with the same spin and two out-of-plane ones with the opposite spin. This, in fact, is the collinear spin structure observed experimentally in KCrF_3 . The obtained Néel temperature is in good agreement with experimental value of 80 K [30], if one takes into account the usual mean-field overestimation of ordering temperatures. Hence one sees that once the orbital order sets in the superexchange is able to account for the value of T_N and observed collinear magnetic structure even without including lattice distortions.⁵

We have also performed the same mean-field calculations with the effective interactions computed with $U = 5.0$ eV, obtaining the same orbitally ordered structure at somewhat lower temperature of 225 K. The obtained low-temperature spin structure is, however, different, it is of the C type and consists of an antiferromagnetic stacking of ferromagnetically ordered [101] plains. Hence each site has two nearest-neighbors with the same spin and four with the opposite one, see Fig. 5(d).

In order to clarify the origin of this change of magnetic order with increasing U , one may carry out a simple estimate of the energy of the A-type and C-type AFM spin structures. First, keeping in (34) only the most important J_{ss} and J_{qq} contributions and summing over all nearest neighbors, one obtains for the mean-field spin-ordering energy (per formula unit, f.u.) of the A-type structure

$$\frac{E_{SO}^{\text{A-type}}}{S^2} = J_{ss} + J_{qq} \left(\langle \hat{\tau}_{iz} \rangle \langle \hat{\tau}_{jz} \rangle - \frac{\sqrt{3}}{2} (\langle \hat{\tau}_{iz} \rangle \langle \hat{\tau}_{jx} \rangle + \langle \hat{\tau}_{ix} \rangle \langle \hat{\tau}_{jz} \rangle) \right), \quad (37)$$

⁴The notation used in Eqs. (35) and (36) follows that used in Ref. [28]. Another representation of the G-type antiferro-orbital order is more standard in the case of LaMnO_3 (see, for example, Ref. [68]) and obtained by substituting θ in (35) and θ_1 in (36) with $\theta/2$ and $-\theta_1/2$, respectively

⁵A possibility for slight noncollinearity as the one present in KCrF_3 between 46 and 80 K was not considered in the mean-field solution of the effective Hamiltonian. Also our simulations neglect the spin-orbit coupling and, hence, are not able to reproduce the spin canting observed below 9 K.

where S^2 is the overall spin factor, which for the case of high-spin Cr^{2+} can be rather well approximated by the square of its classical length, $S^2 = 4$ at the full saturation, i and j label two sublattices of the G-type antiferro-orbital structure. The energy of the C-type structure $E_{SO}^{\text{C-type}}$ is given by the same expression with the minus sign.

The energies of the ferromagnetic (FM) and G-type AFM (all nearest neighbors having the opposite spin) phases are

$$\pm 3S^2 \left(J_{ss} + \frac{J_{qq}}{2} (\langle \hat{\tau}_{iz} \rangle \langle \hat{\tau}_{jz} \rangle + \langle \hat{\tau}_{ix} \rangle \langle \hat{\tau}_{jx} \rangle) \right), \quad (38)$$

where the plus/minus sign is for the FM/AFM case, respectively. One may notice that $\langle \hat{\tau}_{iz} \rangle \langle \hat{\tau}_{jz} \rangle + \langle \hat{\tau}_{ix} \rangle \langle \hat{\tau}_{jx} \rangle$ is always equal to $-1/4$ for the fully saturated G-type antiferro-orbital order and does not depend on the angle θ in Eqs. (35) and (36). Hence, the total energy of the FM and G-type AFM order is also independent of θ .

Assuming a fully saturated G-type antiferro-orbital order, i.e., $\langle \hat{\tau}_{ix} \rangle = \pm \sqrt{1/4 - \langle \hat{\tau}_{iz} \rangle^2}$, $\langle \hat{\tau}_{jx} \rangle = -\langle \hat{\tau}_{ix} \rangle$ and $\langle \hat{\tau}_{jz} \rangle = -\langle \hat{\tau}_{iz} \rangle$, and minimizing (37), one obtains $E_{SO}^{\text{A-type}} = 4J_{ss} - 3J_{qq}/2$ with the orbital state fixed at $\langle \hat{\tau}_{iz} \rangle = \sqrt{3}/4$ and $\langle \hat{\tau}_{ix} \rangle = -1/4$, defined by $\theta = 15^\circ$ in (35). For the C-type structure, one has $E_{SO}^{\text{C-type}} = -4J_{ss} - J_{qq}/2$ and the orbital state locked at $\langle \hat{\tau}_{iz} \rangle = 1/4$ and $\langle \hat{\tau}_{ix} \rangle = \sqrt{3}/4$, corresponding to $\theta = 30^\circ$ (which is, in fact, the experimental orbital state in tetragonal KCrF_3). The energies of the FM and G-type AFM orders do not depend on θ as explained above and are equal to $\pm 3(4J_{ss} - J_{qq}/2)$, respectively. Hence one sees that the spin order is defined by the ratio of J_{qq}/J_{ss} , which increases with decreasing U (increasing J_H/U), see Table I. For $U = 5$ and 3.75 eV, one obtains for the energy difference $E_{SO}^{\text{A-type}} - E_{SO}^{\text{C-type}}$ the values of 2.75 and 0.4 meV per f.u., respectively. Hence at the realistic value of $U = 3.75$ eV those two structures are almost degenerate, though $E_{SO}^{\text{C-type}}$ is still the most stable. The G-type AFM and FM structures are always higher in energy, in particular, for $U = 3.75$ eV their energies are 6.7 and 7.9 meV per f.u. above $E_{SO}^{\text{C-type}}$.

Further analysis shows that the A-type structure is stabilized at $U = 3.75$ eV due to the J_{sq} term, which upon the onset of antiferromagnetism acts as a canting field in the orbital space. For the C-type structure, it takes the form $|J_{qs}|S^2[\langle \hat{\tau}_{iz} \rangle + \langle \hat{\tau}_{jz} \rangle + \sqrt{3}(\langle \hat{\tau}_{ix} \rangle + \langle \hat{\tau}_{jx} \rangle)]$ and one may show that under the corresponding G-type antiferro-orbital order given by $\theta = 30^\circ$, it is not active as long as $J_{qq}S^2 + 8J_{sq}S^2 + 2J_{\tau\tau} > 0$. The system stays in the same antiferro-orbital state with $\theta = 30^\circ$, for which the contribution of the J_{sq} term to the energy is zero. For the A-type structure, it takes the same form with the minus sign, but now under the different orbital state given by $\langle \hat{\tau}_{iz} \rangle = \sqrt{3}/4$ and $\langle \hat{\tau}_{ix} \rangle = -1/4$ ($\theta = 15^\circ$), it does play a role leading to a loss of the perfect G-type antiferro-orbital order. Namely, upon the onset of the A-type spin order the angles θ and θ_1 defining the corresponding orbital states (35) and (36) on two sublattices start deviating from each other, the corresponding loss in the orbital ordering energy is compensated by the ‘‘orbital field’’ due to J_{sq} . The corresponding difference $\Delta\theta = \theta_1 - \theta$ [extracted from mean-field solution of the full effective Hamiltonian, Eq. (34)] grows with decreasing temperature due to increasing spin

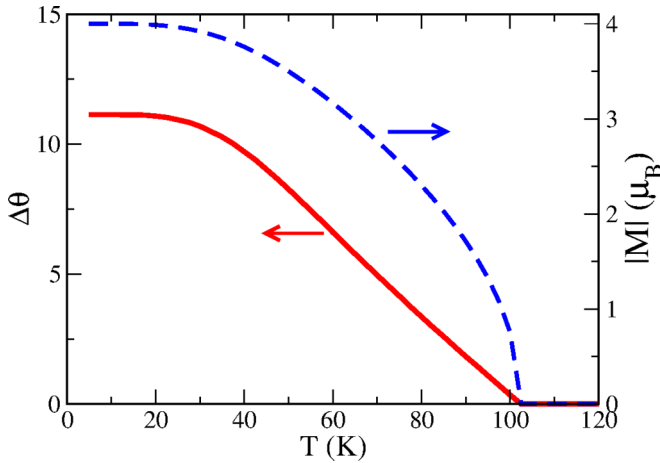


FIG. 6. The spin magnetic moment and orbital misalignment angle $\Delta\theta$ as a function of temperature in the A-type structure obtained for $U = 3.75$ eV.

moment, as shown in Fig. 6. This orbital misalignment stops increasing once the magnetic moment fully saturates below approximately 30 K. The total gain in energy due to this misalignment of about -1.4 meV/(f.u.) is rather small compared to the total energy of the spin-orbital ordering of -22.9 meV/(f.u.), but it is sufficient to stabilize the A-type antiferromagnetic order.

Previously the interplay of orbital ordering and the A-type AFM structure has been intensively studied in the case of the Mn peroxide LaMnO_3 , where Jahn-Teller lattice distortions were proposed to be at the origin of this AFM structure, see, for example, Refs. [23,67,68]. The dependence of the relative stability of different magnetic phases of LaMnO_3 on J_H/U was previously demonstrated in a model study of Ref. [69]. KCrF_3 features some similarities to this system, though in LaMnO_3 the orbital order is of the C-type instead of the G-type. Direct *ab initio* DFT+ U calculations [32,33] for cubic KCrF_3 predicted a ferro-orbital order to be stabilized in conjunction with the A-type AFM, in disagreement with our results and experiment. Apparently, this is due to an incorrect relative scale of spin- and orbital-ordering energies in DFT+ U within the local spin-density approximation, where the orbital order is seen to be induced by the underline AFM state [32]. As one sees from Table I, the interorbital superexchange is the strongest interaction, hence the AFM state emerges well below T_{OO} from an almost completely saturated G-type antiferro-orbital order, in agreement with experiment. In our description, the angle θ , which defines the orbital state (35), is fixed by the lowest-energy AFM order, in real KCrF_3 it is rather fixed by the distorted lattice. The tetragonal distortion favors the C-type AFM in accordance with our calculations, however, experimentally the magnetic order emerges in the lower-temperature monoclinic structure, in which the orbital state is possibly more favorable to the A-type magnetic order. It is interesting to observe that even in the absence of any lattice distortions the feedback effect described above leads to a canted orbital order in conjunction with the A-type AFM. Experimentally, one may also expect to observe an additional small titling/distortion of the CrF_6 octahedra upon the onset

of antiferromagnetism, though our calculations predict a rather small energy scale associated with this process, of the order of 1 meV.

VI. SUMMARY

We have presented a method for computing intersite exchange interactions in correlated materials in the framework of the DFT+DMFT in conjunction with the Hubbard-I approximation to the DMFT self-energy. The expressions for intersite interactions are derived by considering the first-order change in the DFT+DMFT grand potential to simultaneous small fluctuations on two atomic sites with respect to their symmetry-unbroken paramagnetic configuration. The resulting expression (15) combines the variational derivatives of the Hubbard-I self-energy (11) over a given fluctuation in the on-site density matrix with the DMFT intersite Green's functions (16). The method is benchmarked by applying it to the well-known cases of one-band and two-band e_g Hubbard models on the simple-cubic $3d$ lattice.

The presented technique has been already employed to compute spin-spin superexchange interactions in cubic and quasi-two-dimensional tetragonal TM oxides [14]. Here we have applied it to a more complex case of spin-orbital ordering in KCrF_3 in its parent undistorted peroxide structure. We obtained an effective Hamiltonian (34) featuring strong antiferro-orbital nearest-neighbor interactions and a complex anisotropic coupling between orbital and spin moments. By solving it within the mean-field approximation we found the onset of a G-type orbital order at a significantly lower temperature as compared to experiment. In contrast, the appearance of experimentally-observed A-type antiferromagnetic structure is predicted at $T_N = 102$ K in good agreement with experiment. The onset of A-type antiferromagnetism is explained by purely superexchange mechanism as arising due to an interplay of the spin-spin and (spin-orbit)-(spin-orbit) intersite couplings in conjunction with a canting of the G-type antiferro-orbital order. Further applications of this technique to the tetragonal and monoclinic structures of KCrF_3 should help to clarify whether this mechanism for the stabilization of the A-type magnetic structure is qualitatively affected by the lattice distortions.

The present method is promising for applications to a wide range of strongly-correlated materials, like spin-orbital order in TM oxides and fluorides as well as multipolar ordering due to localized f shells in rare-earth and actinide materials. It would be interesting to consider its generalizations beyond the Hubbard-I approximation to widen its range of applicability to materials located close to the Mott point like, e.g., rare-earth nickelates. One might also try to extend the present formalism in order to incorporate contributions to spin-orbital ordering from Jahn-Teller-type distortions.

ACKNOWLEDGMENTS

The author is grateful to A. Georges for his invaluable help in the beginning of this work. J. Mravlje and O. Peil are acknowledged for useful discussions. The author acknowledges the financial support of the Ministry of Education and Science of the Russian Federation in the framework

of Increase Competitiveness Program of NUST MISiS (No. K3-2015-038) as well as computational resources provided

by the National Supercomputer Centre in Linköping (NSC) at Swedish National Infrastructure for Computing (SNIC).

-
- [1] K. I. Kugel' and D. I. Khomskii, *Sov. Phys. Usp.* **25**, 231 (1982).
- [2] R. Shiina, H. Shiba, and P. Thalmeier, *J. Phys. Soc. Jpn.* **66**, 1741 (1997).
- [3] Y. Kuramoto, H. Kusunose, and A. Kiss, *J. Phys. Soc. Jpn.* **78**, 072001 (2009).
- [4] P. Santini, S. Carretta, G. Amoretti, R. Caciuffo, N. Magnani, and G. H. Lander, *Rev. Mod. Phys.* **81**, 807 (2009).
- [5] J. A. Mydosh and P. M. Oppeneer, *Rev. Mod. Phys.* **83**, 1301 (2011).
- [6] V. I. Anisimov, A. I. Poteryaev, M. A. Korotin, A. O. Anokhin, and G. Kotliar, *J. Phys.: Condens. Matter* **9**, 7359 (1997).
- [7] G. Kotliar, S. Y. Savrasov, K. Haule, V. S. Oudovenko, O. Parcollet, and C. A. Marianetti, *Rev. Mod. Phys.* **78**, 865 (2006).
- [8] A. Georges, G. Kotliar, W. Krauth, and M. J. Rozenberg, *Rev. Mod. Phys.* **68**, 13 (1996).
- [9] G. Rohringer, A. Toschi, A. Katanin, and K. Held, *Phys. Rev. Lett.* **107**, 256402 (2011).
- [10] D. Hirschmeier, H. Hafermann, E. Gull, A. I. Lichtenstein, and A. E. Antipov, *Phys. Rev. B* **92**, 144409 (2015).
- [11] T. A. Maier, M. Jarrell, T. C. Schulthess, P. R. C. Kent, and J. B. White, *Phys. Rev. Lett.* **95**, 237001 (2005).
- [12] T. Schäfer, F. Geles, D. Rost, G. Rohringer, E. Arrigoni, K. Held, N. Blümer, M. Aichhorn, and A. Toschi, *Phys. Rev. B* **91**, 125109 (2015).
- [13] T. Ayril and O. Parcollet, *Phys. Rev. B* **92**, 115109 (2015).
- [14] A. Horvat, L. Pourovskii, M. Aichhorn, and J. Mravlje, [arXiv:1501.03033](https://arxiv.org/abs/1501.03033) (unpublished).
- [15] R. E. Prange and V. Korenman, *Phys. Rev. B* **19**, 4691 (1979).
- [16] C. S. Wang, R. E. Prange, and V. Korenman, *Phys. Rev. B* **25**, 5766 (1982).
- [17] T. Oguchi, K. Terakura, and N. Hamada, *J. Phys. F* **13**, 145 (1983).
- [18] T. Oguchi, K. Terakura, and A. R. Williams, *Phys. Rev. B* **28**, 6443 (1983).
- [19] A. Liechtenstein, M. Katsnelson, V. Antropov, and V. Gubanov, *J. Magn. Magn. Mater.* **67**, 65 (1987).
- [20] P. Bruno, *Phys. Rev. Lett.* **90**, 087205 (2003).
- [21] A. V. Ruban, S. Shallcross, S. I. Simak, and H. L. Skriver, *Phys. Rev. B* **70**, 125115 (2004).
- [22] I. V. Solovyev, P. H. Dederichs, and I. Mertig, *Phys. Rev. B* **52**, 13419 (1995).
- [23] I. Solovyev, N. Hamada, and K. Terakura, *Phys. Rev. Lett.* **76**, 4825 (1996).
- [24] M. I. Katsnelson and A. I. Lichtenstein, *Phys. Rev. B* **61**, 8906 (2000).
- [25] S.-T. Pi, R. Nanguneri, and S. Savrasov, *Phys. Rev. Lett.* **112**, 077203 (2014).
- [26] A. Secchi, A. Lichtenstein, and M. Katsnelson, *Ann. Phys.* **360**, 61 (2015).
- [27] J. Hubbard, *Proc. R. Soc. Lond. A* **276**, 238 (1963).
- [28] S. Margadonna and G. Karotsis, *J. Mater. Chem.* **17**, 2013 (2007).
- [29] S. Margadonna and G. Karotsis, *J. Am. Chem. Soc.* **128**, 16436 (2006).
- [30] Y. Xiao, Y. Su, H.-F. Li, C. M. N. Kumar, R. Mittal, J. Persson, A. Senyshyn, K. Gross, and T. Brueckel, *Phys. Rev. B* **82**, 094437 (2010).
- [31] C. Autieri, E. Koch, and E. Pavarini, *Phys. Rev. B* **89**, 155109 (2014).
- [32] G. Giovannetti, S. Margadonna, and J. van den Brink, *Phys. Rev. B* **77**, 075113 (2008).
- [33] M. Xing, X. Liang-Bin, X. Huo-Xi, D. Fei, W. Chun-Zhong, and C. Gang, *Chin. Phys. B* **23**, 037401 (2014).
- [34] L. V. Pourovskii, B. Amadon, S. Biermann, and A. Georges, *Phys. Rev. B* **76**, 235101 (2007).
- [35] S. Y. Savrasov and G. Kotliar, *Phys. Rev. B* **69**, 245101 (2004).
- [36] A. Georges, *AIP Conf. Proc.* **715**, 3 (2004).
- [37] A. R. Mackintosh and O. K. Andersen, in *Electrons at the Fermi Surface*, edited by M. Springford (Cambridge University Press, Cambridge, England, 1980), p. 145.
- [38] I. V. Solovyev and K. Terakura, *Phys. Rev. B* **58**, 15496 (1998).
- [39] T. Plefka, *J. Phys. A: Math. Gen.* **15**, 1971 (1982).
- [40] A. Georges and J. S. Yedidia, *J. Phys. A: Math. Gen.* **24**, 2173 (1991).
- [41] K. Blum, *Density Matrix Theory and Applications* (Plenum Press, New York, 1996).
- [42] O. Parcollet, M. Ferrero, T. Ayril, H. Hafermann, I. Krivenko, L. Messio, and P. Seth, *Comput. Phys. Commun.* **196**, 398 (2015), <http://ipht.cea.fr/triqs/>.
- [43] M. Ulmke, V. Janiš, and D. Vollhardt, *Phys. Rev. B* **51**, 10411 (1995).
- [44] M. Jarrell, *Phys. Rev. Lett.* **69**, 168 (1992).
- [45] R. Strack and D. Vollhardt, *Phys. Rev. B* **46**, 13852 (1992).
- [46] G. Sangiovanni *et al.*, *Phys. Rev. B* **73**, 205121 (2006).
- [47] M. J. Rozenberg, G. Kotliar, and X. Y. Zhang, *Phys. Rev. B* **49**, 10181 (1994).
- [48] A. M. Oleś, L. F. Feiner, and J. Zaanen, *Phys. Rev. B* **61**, 6257 (2000).
- [49] A. Georges, L. de' Medici, and J. Mravlje, *Annu. Rev. Condens. Matter Phys.* **4**, 137 (2013).
- [50] L. F. Feiner, A. M. Oleś, and J. Zaanen, *Phys. Rev. Lett.* **78**, 2799 (1997).
- [51] S. B. Lee, R. Chen, and L. Balents, *Phys. Rev. B* **84**, 165119 (2011).
- [52] H. Park, A. J. Millis, and C. A. Marianetti, *Phys. Rev. Lett.* **109**, 156402 (2012).
- [53] A. Subedi, O. E. Peil, and A. Georges, *Phys. Rev. B* **91**, 075128 (2015).
- [54] P. Hansmann, X. Yang, A. Toschi, G. Khaliullin, O. K. Andersen, and K. Held, *Phys. Rev. Lett.* **103**, 016401 (2009).
- [55] M. J. Han, X. Wang, C. A. Marianetti, and A. J. Millis, *Phys. Rev. Lett.* **107**, 206804 (2011).
- [56] S. Middey, J. Chakhalian, P. Mahadevan, J. Freeland, A. Millis, and D. Sarma, *Annu. Rev. Mater. Res.* **46**, 305 (2016).

- [57] P. Hansmann, A. Toschi, X. Yang, O. K. Andersen, and K. Held, *Phys. Rev. B* **82**, 235123 (2010).
- [58] Y. Ōno, M. Potthoff, and R. Bulla, *Phys. Rev. B* **67**, 035119 (2003).
- [59] A. Rüegg, H.-H. Hung, E. Gull, and G. A. Fiete, *Phys. Rev. B* **89**, 085122 (2014).
- [60] P. Blaha, K. Schwarz, G. Madsen, D. Kvasnicka, and J. Luitz, WIEN2K, An Augmented Plane Wave + Local Orbitals Program for Calculating Crystal Properties (Techn. Universitat Wien, Austria, 2001).
- [61] M. Aichhorn *et al.*, *Comput. Phys. Commun.* **204**, 200 (2016).
- [62] M. Aichhorn, L. Pourovskii, V. Vildosola, M. Ferrero, O. Parcollet, T. Miyake, A. Georges, and S. Biermann, *Phys. Rev. B* **80**, 085101 (2009).
- [63] M. Aichhorn, L. Pourovskii, and A. Georges, *Phys. Rev. B* **84**, 054529 (2011).
- [64] M. Rotter, *J. Magn. Magn. Mater.* **272-276** (Suppl.), E481 (2004), <http://www.mcphase.de/>.
- [65] A. Kokalj, *Comput. Mater. Sci.* **28**, 155 (2003).
- [66] J. Kuneš, R. Arita, P. Wissgott, A. Toschi, H. Ikeda, and K. Held, *Comput. Phys. Commun.* **181**, 1888 (2010).
- [67] H. Sawada, Y. Morikawa, K. Terakura, and N. Hamada, *Phys. Rev. B* **56**, 12154 (1997).
- [68] D. Feinberg, P. Germain, M. Grilli, and G. Seibold, *Phys. Rev. B* **57**, R5583 (1998).
- [69] R. Maezono, S. Ishihara, and N. Nagaosa, *Phys. Rev. B* **58**, 11583 (1998).